CrystEngComm

PAPER

View Article Online
View Journal | View Issue

Cite this: *CrystEngComm*, 2015, **17**, 383

Energetics, thermal isomerisation and photochemistry of the linkage-isomer system [Ni(Et$_4$dien)(η^2-O,ON)(η^1-NO$_2$)]†

Jonathan M. Skelton,‡ Rachel Crespo-Otero,‡ Lauren E. Hatcher, Stephen C. Parker, Paul R. Raithby and Aron Walsh*

Received 8th July 2014,
Accepted 21st August 2014

DOI: 10.1039/c4ce01411a

www.rsc.org/crystengcomm

We present the results of a detailed theoretical study of the linkage isomerisation in [Ni(Et$_4$dien)(η^2-O,ON)(η^1-NO$_2$)] (Et$_4$dien = *N*,*N*,*N*′,*N*′-tetraethyldiethylenetriamine). We probe the structure and bonding of the three experimentally-identified isomers in this system through electronic-structure calculations, and we establish possible transition pathways between them using transition-state modelling and periodic solid-state molecular-dynamics simulations. We also explore the photochemical isomerisation reaction using time-dependent density-functional theory. These results provide a thorough account of the linkage isomerisation in this compound, and add insight to ongoing experimental work on this and related systems.

Introduction

Linkage isomerisation is an interesting phenomenon whereby the binding mode of a ligand to the transition-metal centre in a coordination or organometallic complex changes in response to an external stimulus, typically thermal or photoactivation.[1] Particularly in the solid state, where linkage isomerisation represents a single-crystal-to-single-crystal transition, these systems have attracted much interest. The canonical example, and one of the earliest systems studied, is perhaps sodium nitroprusside (Na[Fe(CN)$_5$(NO)]), in which two long-lived metastable species identified spectroscopically following photoactivation[2–4] were found to correspond to different binding modes of the NO ligand.[5] Since this pioneering work, many more solid-state linkage-isomerisation systems have been found, with two prototypical families of compounds, *viz.* Ni–NO$_2$ (ref. 6–11) and Ru–SO$_2$,[12–15] being widely studied.

Solid-state linkage isomerism can be studied experimentally through single-crystal photocrystallography measurements, in which the crystal is irradiated with light *in situ* on the diffractometer.[1] At low temperatures, the decay of the photoexcited metastable state(s) back to the stable ground state is blocked, allowing them to be characterised through single-crystal X-ray diffraction. Above a certain critical temperature, the so-called metastable limit,[1] the onset of decay back to the ground-state structure occurs. Around the metastable limit, additional short-lived species may be observed in experiments where the crystal is continuously pumped with light during the data collection and thus reaches a "pseudo steady state" population of isomers.[1,10]

A particular challenge from a materials-design standpoint is to engineer the molecular solid so as to obtain a large photoconversion yield while maintaining the reversibility of the transition. In our recent work with linkage isomeric systems, we have chosen to employ a simple crystal-engineering approach, aiming to produce a large "reaction cavity" within which the isomerisation can take place. The reaction cavity serves both to reduce the steric barriers to the transition, and also the stress it places on the crystal.[6,15] Using this design principle, several Ni–NO$_2$ systems with reversible, 100% photoconversion yields have been synthesised.[6,9,10]

[Ni(Et$_4$dien)(η^2-O,ON)(η^1-NO$_2$)] represents a particularly interesting linkage-isomer system because the isomerisation has been shown to be thermally as well as photochemically activated.[7,10] Skeletal structures of the complex and of the three binding modes of the isomerisable NO$_2$ group are shown in Fig. 1. The octahedral Ni centre is coordinated at three sites by the tridentate Et$_4$dien ligand, with another two sites being taken up by an η^2-bound NO$_2$ group. The sixth site is occupied by a second η^1-coordinated NO$_2$ group, the binding mode of which can be switched between three known forms. The N-bound nitro isomer is the stable ground

Department of Chemistry, University of Bath, Claverton Down, Bath, BA1 7AY, UK. E-mail: a.walsh@bath.ac.uk

† Electronic supplementary information (ESI) available: Includes additional calculation results, including the determination of the magnetic ground state of the GS and MS1 crystals, the GS-MS1 enthalpy differences obtained in solid-state and molecular calculations with different parameters, and complete TD-DFT datasets from calculations with several different functionals. See DOI: 10.1039/c4ce01411a

‡ JMS and RCO contributed equally to this work.

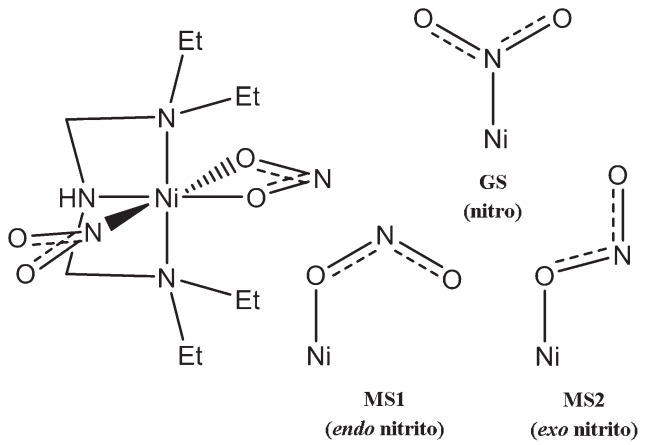

Fig. 1 Schematic structure of the [Ni(Et_4dien)(η^2-O,ON)(η^1-NO_2)] system. The four skeletal drawings show the structure of the molecule (left) and the three different binding modes of the isomerisable NO_2 group (right), *viz.* the ground-state (GS) nitro and metastable *endo*- and *exo*-nitrito forms (MS1/MS2, respectively).

state (GS), and is formed by cooling in the absence of illumination. The metastable O-bound *endo*-nitrito isomer (MS1) can be generated from the GS complex by photoactivation at 100 K and, additionally, can be generated thermally in significant population at higher temperatures.[7] More recently,[10] a second O-bound *exo*-nitrito isomer (MS2) was observed in pseudo-steady-state photocrystallographic experiments at temperatures close to the metastable limit of ~150–160 K, which indicates that this species has a lifetime that is shorter than the duration of the X-ray data collection.

While the steady-state structures of the various isomers in this system have been well characterised, little is presently known of the transition pathways which connect them. In this respect, the thermal isomerisation exhibited by this system makes it an ideal candidate for theoretical investigation. Whereas exploring excited-state potential-energy surfaces can pose a significant challenge for quantum chemistry, characterisation of ground-state properties is much less difficult. An understanding of the thermal isomerisation pathways could then, in principle, provide a basis for modelling the photochemical reaction.

In this article, we present the results of a computational study of the linkage isomerisation in [Ni(Et_4dien)(η^2-O,ON)(η^1-NO_2)], using a combination of solid-state and molecular quantum-chemistry calculations. We perform detailed electronic-structure calculations on the three species, and identify the isomerisation pathways connecting them using transition-state modelling and solid-state molecular dynamics. We also show that the crystal environment significantly influences the energetics of the isomerisation. Finally, we present some preliminary data from ongoing photochemical modelling, which provides some insight into possible excited-state isomerisation pathways. Our modelling provides important theoretical insight into the dynamics of linkage isomerisation in this system, and will support ongoing experimental work on this and related materials.

Computational methods

All computational modelling was carried out within the Kohn–Sham density-functional theory (DFT) formalism.[16] Models of the ground- and metastable-state crystal structures were created from the crystallographic data published with ref. 7. For the molecular quantum-chemistry calculations, single complexes were extracted from these published structures, and an initial model of the MS2 complex was made from the MS1 structure by rotating the O-bound NO_2 ligand. Separate software packages were used for the solid-state and molecular calculations, as outlined below.

Periodic solid-state calculations

DFT calculations with periodic boundary conditions were carried out using the VASP code.[17] The semi-local PBEsol exchange-correlation functional[18] was used for the majority of the calculations, although we also tested several other functionals, *viz.* PBE,[19] the semi-empirical dispersion-corrected PBE-D2[20] and PBE-D3[21] functionals, and the non-local vdw-DF[22] and vdw-DF2[23] functionals. Projector-augmented wave pseudopotentials[24] were used, and the Brillouin zone was sampled at the Γ point. A plane-wave cut-off of 944.5 eV was used during geometry optimisations and single-point calculations, and molecular-dynamics (MD) simulations were performed with a smaller cut-off of 755.6 eV. As described in the results section, a Hubbard *U* correction of 5.32 eV was applied to the Ni d bands during the MD simulations, using the scheme of Dudarev *et al.*[25] For these calculations, non-spherical contributions to the gradient corrections within the PAW spheres were accounted for.

Geometry optimisation was performed by allowing the atomic positions to relax until the magnitude of the forces on the ions was less than 10^{-2} eV Å^{-1}. After convergence, we found that with PBEsol the stress on the simulation cell was less than 0.2 GPa in both models, so we opted to fix the volume and cell shape at the experimentally-determined parameters. MD simulations were carried out with the constraint that only the isomerisable NO_2 ligands be allowed to move; by fixing the lighter atoms, we were then able to use a relatively long integration timestep of 5 fs. A Berendsen thermostat[26] was used to fix the temperature during the dynamics simulations.

Molecular calculations

All isolated molecular calculations were performed using Gaussian09 program.[27] A range of different functionals were employed for studying energetics, *viz.* PBE,[19] the PBE0,[28] B3LYP,[29]and TPSSH[30] hybrid functionals, the M06 meta-hybrid,[31] and the CAMB3LYP long-range-corrected hybrid.[32] The M06 and PBE0 functionals were used for the transition-state and photochemistry modelling, due to their good general-purpose performance when describing a broad range of properties.[33] Triplet and singlet states were computed

using the unrestricted and restricted approaches, respectively. The LANL2DZ basis set and corresponding pseudopotential were used to treat the Ni atom, with various combinations of the split-valence 6-31G(p), 6-311G(d) and 6-311++G(d,p) basis sets being used for the lighter atoms. Polarisable continuum model (PCM) calculations, carried out to study the possible effects of the crystal environment on properties,[34] were performed to mimic three different solvents with increasing dielectric constants, *viz.* toluene (ε = 2.4), ethanol (ε = 24.9) and water (ε = 78.4).

Transition-state modelling calculations were performed in the gas phase with the 6-31G(d) and 6-311++G(d,p) basis sets and the M06 and PBE0 functionals. Calculations with water as a polarisable continuum were performed using the 6-31G(d) basis set for geometry optimisation, and the 6-311++G(d,p) basis set for single-point energy calculations. Harmonic vibrational-frequency calculations were performed to confirm the nature of all stationary points found, and Intrinsic Reaction Coordinate (IRC) calculations[35] were carried out to check the connection between the reactants, transition states and products.

To study the photochemistry of the complexes, time-dependent DFT (TD-DFT) calculations on both the triplet and singlet excited states were carried out, using the corresponding triplet and singlet ground-state wavefunctions as references. Different functionals, *viz.* M06,[31] B3LYP,[29] PBE0,[28] M06HF[36,37] and wB97xd[38] were considered in combination with the LANL2DZ pseudopotential and basis set for Ni, with a 6-311++G(d,p) basis set being used for the light atoms (this mixed basis set is referred to as LANL2DZ/6-311++G(d,p) in the text). The TD-DFT calculations were performed with water as a polarisable continuum.

Results and discussion

Energetics and ground-state magnetism

Solid-state calculations. To explore the energetics and magnetic properties of the system, we first performed a series of single-point calculations on the optimised GS and MS1 crystal structures. The Ni atom in both complexes is formally Ni(II) in an octahedral environment, and thus a simple crystal-field model of the d-orbital splitting would predict two unpaired electrons in the e_g orbitals. We found that this open-shell magnetic state was the lowest-energy in both structures, with energy differences of ΔE_{T-S} = −35.4 and −39.0 kJ mol^{-1} per molecule in the GS and MS1 isomers, respectively. For comparison, these are both considerably larger than the difference in energy between the isomers themselves, which for the triplet states was calculated to be ΔE_{GS-MS1} = −23.9 kJ mol^{-1} per molecule.

Given that the crystal structures are formed of essentially isolated complexes, one would not expect long-range magnetic interactions to occur between the Ni centres. To confirm this, we compared the relative energies of a ferromagnetic state, with all the Ni magnetic moments aligned in the same direction, and three different antiferromagnetic states with the moments on different pairs of Ni atoms oriented in opposite directions. We found no significant difference in energy between these configurations; the maximum 0.08 kJ mol^{-1} per molecule is well within the error of the calculations.

To compare the calculated GS–MS1 energy difference against experiment, we fitted the temperature dependence of the isomer populations reported in ref. 7 to a Boltzmann expression, which yielded an enthalpy difference of 9.69 kJ mol^{-1} per molecule (see ESI†). This value is less than half the difference computed in these calculations, and so we therefore opted to investigate briefly the effect of some computational parameters on the computed ΔE.

Given that the Ni centre is a central component in the isomerisation process, it is possible that the discrepancy arises from common issues which (semi-)local DFT functionals can encounter when treating strongly-correlated 3d-electrons.[39] We therefore investigated the effect of applying a Hubbard U correction to the Ni d states on the energy difference between the two structures. Strikingly, we found that the difference reduced systematically with the magnitude of the U term (see ESI†), such that for a value of 5.32 eV the experimental enthalpy difference was reproduced to within 0.2 kJ mol^{-1}. The size of this correction is reasonable, and is not too dissimilar to, for example, the typical values used in DFT + U calculations on NiO in the literature (*e.g.* ref. 25 and 40). We also note in passing that extrapolating the trend suggests that a larger on-site potential of around 10 eV would zero the energy difference between the isomers. Finally, it is worth mentioning that while, in the present case, the U correction was chosen to match experimental data, as is fairly common practice, an alternative, a less empirical linear-response method exists to obtain the value from first-principles;[41] however, this technique is not presently implemented in VASP.

A second factor which may play an important role in the energetics is dispersion, another effect which many DFT functionals struggle to describe accurately, and which is likely to be significant in molecular crystals such as this. The PBEsol functional does not include any explicit dispersion corrections, and so to quantify the differences such corrections might make we performed additional geometry optimisations on the GS and MS1 crystals using a selection of other functionals, *viz.* PBE,[19] PBE-D2[20] and PBE-D3,[21] and vdw-DF[22] and vdw-DF2.[23] The D2/D3 functionals apply a semi-empirical correction to the PBE energies to approximately account for dispersion interactions, while the vdw-DF functionals are non-empirical and attempt to treat dispersion more accurately through a non-local electron correlation. After geometry optimization, we compared the calculated GS–MS1 energy differences, and also various bond lengths around the Ni centre, between the six functionals to experimental data (see ESI†). We found that the energy differences computed with PBE and the two vdw-DF functionals came closest to the experimental values, whereas the dispersion corrections applied by the PBE-D2/D3 methods yielded values similar to PBEsol; however, in all cases the difference

was consistently overestimated. The better match of the computed energy difference with experimental data obtained with the vdw-DF functionals might be taken as an indication that dispersion forces make a significant contribution to the energetics, although this should be a tentative conclusion, since it is quite possible that the dispersion corrections in these functionals may be compensating for other issues, *e.g.* the aforementioned inability of standard DFT functionals to treat the correlated Ni 3d electrons.

However, bearing this caveat in mind, these two sets of tests suggest that to accurately capture the energetics of this system requires both a good description of the Ni d electrons, and also accounting for dispersion forces.

An important question about the isomerisation process is whether or not it proceeds in a concerted manner, *i.e.* whether one complex isomerising influences subsequent events at neighbouring sites. To investigate this, we created variants of the GS and MS1 crystal structures in which 1–4 of the η^1-bound NO_2 ligands were swapped with their isomers "by hand", thereby converting 1–4 of the symmetry-equivalent molecular complexes to the other isomer. The geometries of these models were then optimized with PBEsol, and, after verifying that the isomerisation was not reversed, we compared the energy change from flipping 1–4 of the ligands in tandem against the sum of the energy required to flip the same ligands in isolation (Fig. 2a).

For the GS-to-MS1 isomerisation, up to three flips (75% conversion) leads to a change in energy which is more or less equal to the sum of those for the individual isomerisations, whereas the fourth leads to a disproportionately large relative increase in energy. We observed a linear increase in the stress on the unit cell with successive isomerisations (Fig. 2b), which is consistent with the fact that the MS1 structure has a larger unit-cell volume than the GS one. If this build-up of stress makes the final isomerisation energetically more difficult, one might infer that, during very fast (*e.g.* laser-induced) photoisomerisation processes, the final 25% conversion may be constrained by lattice relaxation (phonon coupling). In keeping with this picture, we found that for the reverse MS1-to-GS transition, where isomerisation leads to a negative stress, the energy required to flip all four ligands was practically identical to the sum of the individual isomerisation energies. These results thus suggest that, at equilibrium, the isomerisation is not a concerted process, in either direction, and is likely to happen randomly throughout the crystal. This is consistent with kinetic data from photocrystallographic measurements.[10]

Molecular calculations. The solid-state calculations suggest that, to a good approximation, the molecular units behave as isolated complexes, influenced by the dielectric environment of the crystal. We therefore carried out molecular quantum-chemistry calculations on complexes extracted from the GS and MS1 crystal structures, plus a model of the MS2 intermediate obtained by rotating the O-bound NO_2 group in MS1.

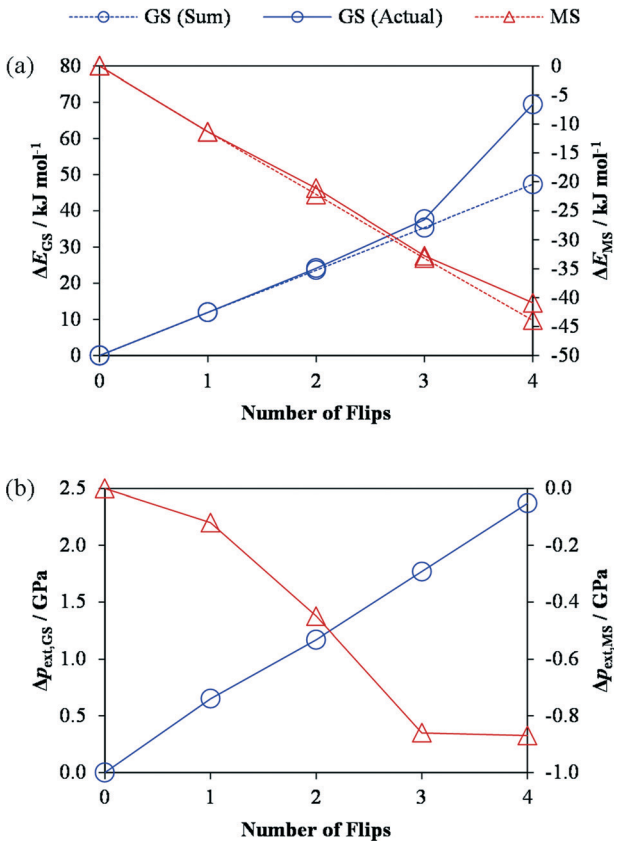

Fig. 2 Effect of the GS → MS1 (blue line) and reverse MS1 → GS (red line) isomerisation on the energy of (a) and external pressure on (p_{ext}; b) the GS/MS1 crystal structures. In plot (a), the sum of the energy changes which occur when 1–4 ligands are isomerised in isolation (dashed lines) is compared against the energy change on flipping the same number of ligands in tandem. The energies and stresses are computed from single-point PBEsol + *U* calculations performed on the PBEsol-optimised structures. These calculations suggest that the linear increase in the stress on the unit cell with conversion during the GS → MS1 transition makes the final isomerisation energetically more difficult, in the absence of lattice relaxation.

The relative energy differences between the three species, calculated using various functionals and basis sets, are collected in Table 1. Corresponding energy differences between MS1 and MS2 may be found in Table 2. Interestingly, MS1 is found to be lower in energy than the GS in the gas phase for all the combinations considered, save for PBE/LANL2DZ/6-311G(d) (ΔE_{GS-MS1} = −13 kJ mol^{-1}), which suggests that PBE may exhibit some favourable error compensation. To investigate this further, we created periodic molecular models of the GS and MS1 complexes, by placing the molecules in a simulation cell with a large vacuum gap to separate them from adjacent periodic images. After converging the energy as a function of the gap size and optimizing the geometry with PBEsol, we obtained an energy difference of ΔE_{GS-MS1} = −14.6 kJ mol^{-1} per molecule (see ESI†). Single-point calculations with a Hubbard *U* correction of 5.32 eV and with the bare PBE functional yielded energy differences of −1.4 and −9.3 kJ mol^{-1}, respectively. The reasonably good correspondence between the

Table 1 Calculated energy differences between the GS and MS1 complexes (ΔE_{GS-MS1}). The entries compare, variously, the effect of different exchange-correlation (XC) functionals, basis sets and polarisable dielectric continuums on the energies of the two isomers. In tests where a pseudopotential was used to describe the Ni core electrons, the first entry in the basis-set column gives the basis used for the Ni atom, and the second gives that used for all other atoms

XC functional	Basis set	Continuum	ΔE_{GS-MS1}/kJ mol^{-1}
PBE	LANL2DZ/6-31G(d)	None	2.45
PBE0		None	11.7
B3LYP		None	15.70
TPSSH		None	9.71
M06		None	9.33
CAMB3LYP		None	19.70
PBE	LANL2DZ/6-311G(d)	None	−13.01
PBE0		None	6.03
M06		None	1.62
M06	6-311G(d)	None	2.39
M06	LANL2DZ/6-311+	None	1.84
M06	+G(d,p)	PhMe	−1.81
M06		EtOH	−6.96
M06		H_2O	−7.54

latter value and the molecular calculations suggests that the 6-311G(d) basis set used in the latter is approaching the convergence limit with respect to this property.

For PBE, PBE0 and M06, ΔE_{GS-MS1} becomes more negative as the basis set size is increased, although even with the largest basis sets the latter two still predict an incorrect relative ordering. Comparing the PBE0, TPSSH and PBE functionals, which notionally have decreasing exchange-energy contributions, the energy difference is seen to decrease; this is similar to the effect of including the *U* correction in the periodic PBEsol calculations, and illustrates that the exchange potential makes an important contribution to the energy difference between the isomers.

To obtain the correct size of the energy difference between the isomers, we found that the basis set for the lighter elements needed to be of at least triple-zeta quality, while for the metal the use of the LANL2DZ basis set and pseudopotential did not affect significantly the results, leading to a change in ΔE_{MS1-GS} of only 0.6 kJ mol^{-1} with the M06 functional. To obtain the correct sign of ΔE_{GS-MS1}, a combination of a triple-zeta basis set for the light elements and the continuum solvent model was needed. With the M06 functional in combination with the 6-311++G(d,p) basis set, PCM simulations with the dielectric constant of toluene, ethanol and water gave ΔE_{GS-MS1} values of −1.81, −6.96 and −7.54 kJ mol^{-1}, respectively.

Table 2 Calculated energy differences between the MS1 and MS2 complexes ($\Delta E_{MS2-MS1}$). These entries compare the values obtained for two different DFT functionals, *viz.* M06 and PBE0, in the gas phase and with water as a polarisable continuum

XC functional	Basis set	Continuum	$\Delta E_{MS2-MS1}$/kJ mol^{-1}
M06	LANL2DZ/6-311G+	None	14.31
M06	+(d,p)	H_2O	4.83
PBE0		None	8.69
PBE0		H_2O	0.86

We note that differences in vibrational zero-point energy are not expected to affect significantly the relative stabilities of the species; energy corrections estimated within the harmonic approximation at the M06/LANL2DZ/6-31G(d) level of theory change ΔE_{GS-MS1} by less than 1 kJ mol^{-1} (ΔE + ZPVE = 8.76 kJ mol^{-1}, compared to ΔE = 9.33 kJ mol^{-1}).

We now consider the optimised geometries of the molecular complexes. Fig. 3 shows the geometry in the plane defined by the nitro ligands and the Ni centre in the GS, MS1 and MS2 isomers. Comparing with available experimental data (see ESI†), the agreement between the bond lengths in the optimised complexes and the crystal structures is generally very good, with the only exception being a significant underestimation of the length of the O(η^1-NO_2)–HN distance. We note that a crystal structure containing the MS2 geometry was not available to compare this set of data against.

The main difference between the GS and MS1 isomers lies in the relative stabilities of the Ni–N and Ni–O bonds. A Natural Bond Orbital (NBO) second-order perturbation analysis[42] shows that the most important stabilisation of both bonds is through electron transfer from the ligand to the metal. The Ni–N bond is more energetically favourable by around 9 kJ mol^{-1} due to the better donor capacity of N ($\Delta^2E_{LP(N)\rightarrow Ni}$ = 160 kJ mol^{-1}, $\Delta^2E_{LP(O)\rightarrow Ni}$ = 151 kJ mol^{-1} at the M06/6-311++G(d,p) level with a continuum of water).

An additional source of stabilisation is the weak hydrogen bond between the ligand O atom and the NH group on the Et_4dien molecule (classified as such based on intermolecular distance criteria[43]). The effect of this interaction is most pronounced in the gas phase; the presence of a solvent increases the O–H–N distances, leading to a consequent weakening of the interaction due to dielectric screening. Comparing the hydrogen-bond distances between the isomers, we obtain 2.01–2.21 and 1.93–2.05 Å in the GS and MS1 complexes, respectively, depending on the level of theory.

As in MS1, the coordination of the NO_2 group to Ni in the MS2 complex is through O. However, due to the geometry of the ligand, the hydrogen-bonding interaction occurs *via* N, and the length is comparable to the bond in the GS complex, making it weaker than the bond in the MS1 isomer. As a result of the effect of a dielectric medium on the hydrogen-bonding interaction, the energy difference between MS1 and MS2 is reduced significantly when a polarisable continuum is included in the calculations, ranging from $\Delta E_{MS2-MS1}$ = 18.72 kJ mol^{-1} in the gas phase to 4.83 kJ mol^{-1} in water using the M06 functional, and from 8.69 to 0.86 kJ mol^{-1} with PBE0.

In summary, these calculations suggest that the energy differences between the three linkage isomers is governed by a combination of the influence of the ligand on the Ni 3d states, and hydrogen-bonding interactions between the ligand and the N–H group on the Et_4dien ligand. Whether modelled explicitly or implicitly, it is apparent that the crystalline environment significantly influences the relative energies of the three isomers compared to in the gas phase.

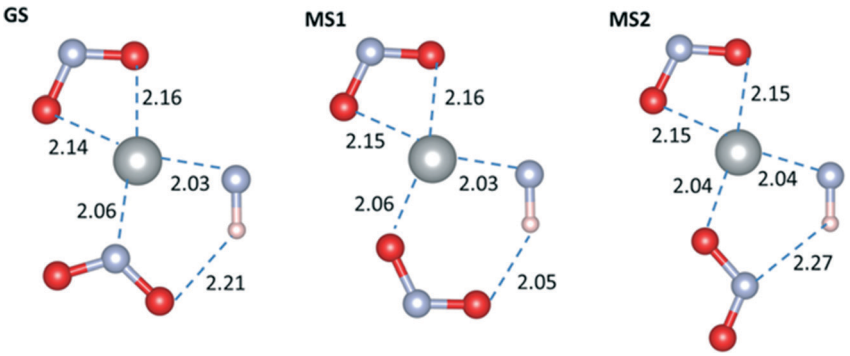

Fig. 3 Optimised geometries of the GS, MS1 and MS2 complexes with the M06 functional and the LANL2DZ/6-311++G(d,p) basis set, with water as a dielectric continuum.

However, this appears to be largely a dielectric effect, as the periodic calculations suggest a minimal interaction, if any, between complexes in the molecular crystal; this observation extends to the isomerisation process itself, as the present calculations confirm the experimental finding that the isomerization is likely to be a random, rather than a concerted, process. The pronounced effect that the crystal environment has on the isomerization energetics reinforces the idea that crystal engineering, *e.g.* tuning the size of the "reaction cavity", could be used to control the switching process, as has already been discussed in relation to a number of linkage-isomer systems.[6,15]

Thermal isomerisation: molecular calculations. The main difference between the GS, MS1 and MS2 isomers is the position of the NO_2 group. Considering the plane formed by the Ni atom and the isomerisable NO_2 group, the three isomers can be connected by simple rotations of the ligand either in or out of this plane. Hypothetical GS-to-MS1/2 isomerisations would also require the breaking or weakening of the bonds between N/O and Ni. The symmetry of the complex is such that, for each process, two similar transition states may be relevant – indeed, in general both possibilities were found to be saddle points on the potential energy surfaces, albeit with similar energies. Fig. 4 illustrates the transition states connecting the GS, MS1, and MS2 structures, labelled TS1/TS2 and MTS1/MTS2, respectively; the corresponding energies, computed with M06 and PBE0 and the LANL2DZ/6-311++G(d,p) basis set, are listed in Table 3.

TS1 and TS2 correspond to the rotation of the NO_2 group up and down with respect to the plane, respectively. The energy barriers for these processes, computed at the M06/LANL2DZ/6-311++G(d,p) level of theory, are both around 70 kJ mol^{-1}, and the presence of water as a continuum increases both barrier heights by roughly 10 kJ mol^{-1}. With the PBE0 functional, both barriers are reduced.

The transition states connecting MS1 and MS2, labelled MST1 and MST2, are (anti)clockwise rotations of the ligand about the Ni–O bond. In both the gas phase and continuum calculations, and for both the M06 and PBE0 functionals, the two were found to have very similar energies and geometries. While these transition states are superficially similar to TS1 and TS2, the Ni–O bond length remains constant between MS1 and MS2, indicating that this O remains bonded during the rotation; consequently, the MS1-to-MS2 isomerisation requires roughly half the energy of the GS-to-MS1 conversion.

We also explored possible direct isomerisation pathways between the GS and MS2 isomers by a relaxed scan of the Ni–O–N angle in the Ni–O_2N plane. This yielded a continuous increase in energy, with no further stabilisation. When intermediate geometries were optimised as transition states, an additional transition state, TS3, was found (see ESI†), but IRC calculations indicated that this does not connect GS and MS2; rather, this transition state appears to be an in-plane rotation of the O_2N ligand connecting two further high-energy metastable structures which have not been observed experimentally. Whether these structures represent transient species (*e.g.* detectable in ultrafast laser-excitation experiments), or are merely artifacts, is presently unclear.

The kinetic measurements reported in ref. 10 yielded an activation barrier for the decay of MS1 to the GS of 48.6 kJ mol^{-1}, which is closer to the calculated barrier for the MS1-to-MS2 transition than to the MS1-to-GS one. In the absence of a direct GS-to-MS2 isomerisation pathway, this would suggest that the calculated barriers for the GS-to-MS1 transition have been overestimated considerably. However, if a GS-to-MS2 path did exist, and had an activation barrier lower than that for the MS1-to-MS2 transition, then the rate-limiting step in the decay would then be the MS1 → MS2 isomerisation, and the calculated barrier for this is much closer to the experimental value. With regard to the accuracy of the calculated barriers, it is worth noting that the functional, basis set and continuum were optimised to reproduce only the enthalpy differences, and not necessarily the transition barriers. Moreover, since the energetics in this system are evidently quite sensitive to the continuum, it is possible that the use of the high dielectric constant of water in the PCM model may be compensating for deficiencies in either or both of the functional or basis set.

To investigate this further requires the calculation or measurement of the macroscopic dielectric constant of the crystal, which is the subject of ongoing work.

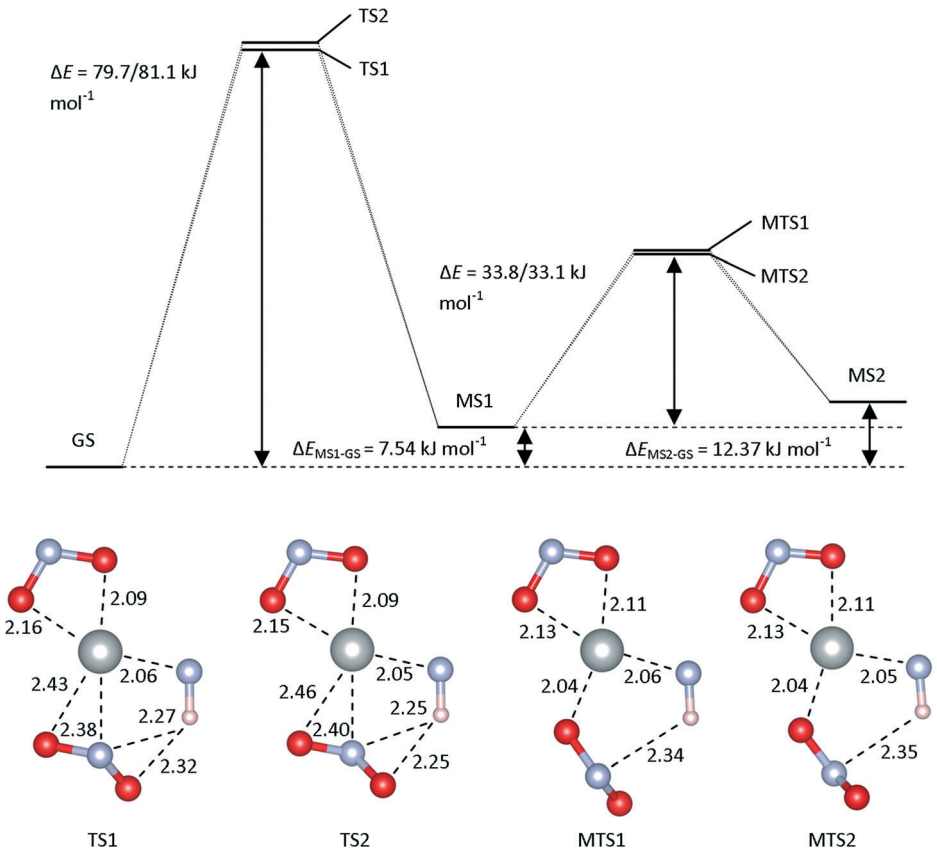

Fig. 4 Schematic of the isomerisation pathways in [Ni(Et$_4$dien)(η^2-O,ON)(η^1-NO$_2$)], modelled using the M06 functional and the LANL2DZ/6-311++G(d,p) basis set, and with water as a continuum. The energy profile illustrates the relative energies of the GS, MS1 and MS2 isomers, and the transition states connecting them, while the four models show the optimised geometries of the four transition states.

Table 3 Energy barriers for the formation of the most important transition states between the GS and MS1 isomers (TS1, TS2) and the MS1 and MS2 isomers (MTS1, MTS2). For each transition state, the barrier height has been computed with the PBE0 and M06 functionals using the LANL2DZ/6-311++G(d,p) basis set, and with and without water as a continuum

Species	Continuum	ΔE_{PBE0}/kJ mol^{-1}	ΔE_{M06}/kJ mol^{-1}
TS1	None	66.3	71.4
	H_2O	60.7	79.7
TS2	None	66.6	70.8
	H_2O	68.1	81.1
MTS1	None	31.2	35.9
	H_2O	32.2	33.8
MTS2	None	31.1	35.1
	H_2O	33.8	33.1

In spite of these potential issues, the present calculations establish an intuitive isomerization pathway between the three isomers. The isomerisation between MS1 and MS2 has a (relatively) low activation energy, which would allow equilibration between them over a range of temperatures, and, as found from the energetics calculations, MS1 is the more stable of the two. This low thermal barrier to conversion between the *endo* and *exo* isomers naturally explains the observation of the latter as a transient intermediate in a narrow temperature range – when the system is heated close to the relatively low-temperature metastable limit, the MS1-to-MS2 isomerisation will be accessible, but slow (on crystallographic data-collection timescales), resulting in a small but detectable steady-state population of the MS2 state.

Solid-state molecular dynamics. Given the apparent importance of the crystalline environment, we performed short (50 ps) constrained periodic molecular-dynamics (MD) simulations on the MS1 structure at 370 K, being the highest of the temperatures investigated experimentally in ref. 7, to see whether we could observe the transition pathways found in the molecular calculations. The energy and forces were calculated using the PBEsol functional, with a Hubbard U correction of 5.32 eV, as discussed in the section on energetics; we opted for this combination as an inexpensive means of reproducing the experimental enthalpy difference between the GS and MS1 isomers. While we were not able to observe the MS1-to-GS isomerisation over this timescale, we did observe both the MS1-to-MS2 and the reverse MS2-to-MS1 transitions. To obtain energy profiles for these processes, we extracted the configurations of the isomerisable NO_2 group during the transition and performed a series of single-point total-energy calculations while keeping the other three groups fixed at their initial positions. Fig. 5 shows the energy profile for the MS1-to-MS2 transition, together with snapshots of the complex at different points on the curve; a profile for the reverse MS2-to-MS1 isomerisation may be found in the ESI.†

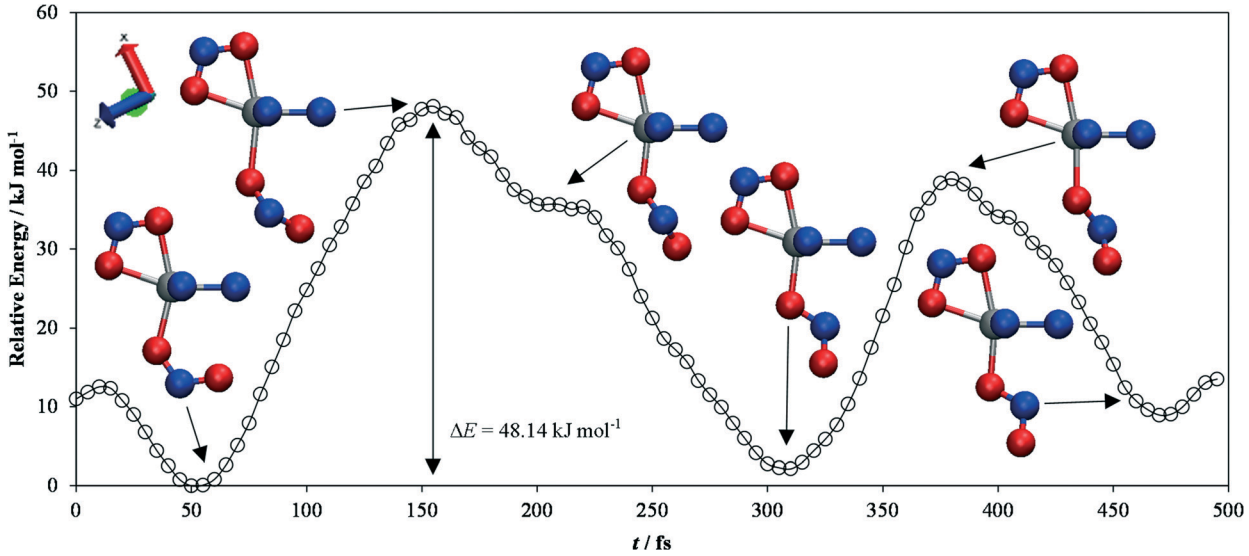

Fig. 5 Energy profile for the *endo*-to-*exo* transition in [Ni(Et_4dien)(η^2-O,ON)(η^1-NO_2)], obtained from constrained *ab initio* molecular-dynamics simulations. The energies are expressed relative to the lowest-energy point on the curve. Snapshots of the geometry of the complex at various local maxima and minima on the profile are shown, with the atoms colour coded as follows: N – blue, O – red, Ni – silver. The largest energy barrier involved in the switching is 48.14 kJ mol^{-1}, and corresponds to a clockwise rotation of the NO_2 group by approximately 45° from the *endo* position. The snapshots were created with the VMD software.[44]

This analysis suggests that the largest energy barrier in the switching process is the point at which the ligand is rotated by ~45° with respect to the plane in which it sits in the *endo*/*exo* positions.

This configuration is around 12.2 kJ mol^{-1} higher in energy than the one with the ligand at 90°, although the latter is still a local energy maximum. Indeed, a second position with the ligand at 45° to the *endo*/*exo* plane is also an energy maximum, and in this particular trajectory appears to block the ligand from making a complete rotation when it falls from the transition state to the local *exo* minimum.

The overall barrier height for the *endo*-to-*exo* transition is ~48 kJ mol^{-1}, and the energy difference between the *endo* and *exo* forms is $\Delta E_{MS2-MS1}$ = 2.13 kJ mol^{-1}. The discrepancy between these results and those from the molecular calculations is most likely due in part to the use of the semi-local PBEsol functional, as opposed to the more sophisticated (meta)hybrids available for molecular calculations, plus the fact that a large part of the structure was constrained to the initial MS1 geometry, thus preventing the rest of the molecular backbone relaxing during the transition.

However, the fact that the same transition states connecting MS1 and MS2 as were observed in the molecular calculations are seem in the MD calculations – in which the system is able to explore its potential energy surface more fully – serves as a powerful validation of the mechanism established from the former.

The photochemical process: excited states. The [Ni(Et_4dien)(η^2-O,ON)(η^1-NO_2)] system studied here is unique in that its isomerisation is both thermally and photochemically activated. Although the former is the main focus of this work, it is of interest to see how photoexcitation may influence the thermal reaction pathway established from the transition-state calculations.

The experimentally-reported UV-visible spectrum of the GS complex in ref. 10 shows an intense absorption band around 400 nm (3.1 eV), and we would hence expect to predict a significant absorption in this spectral region from the molecular calculations, given a suitable choice of polarisable continuum. However, the prediction of accurate absorption energies and oscillator strengths represents a significant challenge for computational chemistry,[45,46] and for most of the levels of theory considered in this work the first excited state with significant intensity appears at much higher energies; only M06 and B3LYP predict bands with significant oscillator strengths (around 0.02) close to the correct spectral region (3.64 and 3.82 eV, respectively). The most important excited states, at the TD-M06/LANL2DZ/6-311++G(d,p) level of theory with water as a continuum, are listed in Table 4. We show only the excited states that could be relevant for the photoisomerisation process, but the complete TD-DFT dataset, including the transitions obtained with all the functionals tested, may be found in the ESI.†

The main orbitals involved in the transitions in the GS isomer are shown in Fig. 6. The first six triplet excited states (T_1 to T_6) in both the GS and MS are transitions between the $HOMO^{\beta}$–5/$HOMO^{\beta}$–6 and $LUMO^{\beta}$/$LUMO^{\beta}$+1 orbitals; the orbital labelling is based on the beta spin channel (that which does not contain the two unpaired electrons) in which we found the most important calculated transitions took place. These electronic excitations all involve a redistribution of the electron density over the NO_2 ligands and the metal, and as such can be assigned as delocalized metal-to-ligand (ML) transitions.

$HOMO^{\beta}$–5 contains an important contribution from the Ni d_{xz} and ONO (static ligand) p_x orbitals, while $HOMO^{\beta}$–6 is made up of the Ni d_{xy} and NO_2 (isomerisable ligand) p_x orbitals. The $LUMO^{\beta}$ and $LUMO^{\beta}$+1 orbitals have anti-bonding contributions between the Ni d orbitals in the *yz*

Table 4 Triplet excited states calculated at the TD-DFT/M06 level with the LANL2DZ/6-311++G(d,p) basis set and water as a polarisable continuum; the ground-state reference was the triplet electronic ground state. Each state is listed together with its corresponding calculated oscillator strength, and is assigned as either a metal-to-ligand delocalised (ML) or a metal-to-ligand charge-transfer (MLCT) state. The left portion of the table lists the excited states computed for the GS molecule (prefixed "GS"), while the right portion lists states computed for the MS1 isomer (prefixed "MS1")

State	*E*/eV (nm)	Oscillator strength	Assignment	State	*E*/eV (nm)	Oscillator strength	Assignment
GS-T_1	0.98 (1260)	0.0002	ML	MS1-T_1	1.01 (1230)	0.0000	ML
GS-T_2	1.01 (1230)	0.0001	ML	MS1-T_2	1.08 (1145)	0.0000	ML
GS-T_3	1.08 (1145)	0.0000	ML	MS1-T_3	1.55 (799)	0.0003	ML
GS-T_4	1.55 (799)	0.0002	ML	MS1-T_4	1.65 (752)	0.0000	ML
GS-T_5	1.65 (752)	0.0000	ML	MS1-T_5	1.82 (682)	0.0002	ML
GS-T_6	1.82 (682)	0.0001	ML	MS1-T_6	2.73 (455)	0.0001	ML
GS-T_7	2.73 (455)	0.0002	MLCT (NO_2)	MS1-T_7	2.88 (431)	0.0000	MLCT (NO_2)
GS-T_8	2.88 (431)	0.0000	MLCT (O_2N)	MS1-T_8	3.41 (363)	0.0000	MLCT (O_2N)
GS-T_9	3.41 (363)	0.0073	ML	MS1-T_9	3.61 (343)	0.0015	MLCT (NO_2)
GS-T_{10}	3.61 (343)	0.0005	MLCT (NO_2)	MS1-T_{10}	3.64 (340)	0.0197	ML
GS-T_{11}	3.64 (340)	0.0376	ML	MS1-T_{11}	3.67 (338)	0.0218	ML
GS-T_{12}	3.67 (338)	0.0205	ML	MS1-T_{12}	3.73 (332)	0.0011	ML
GS-T_{17}	3.98 (312)	0.0238	ML	MS1-T_{15}	3.98 (312)	0.0379	ML
GS-T_{18}	4.02 (309)	0.1216	ML	MS1-T_{16}	4.00 (310)	0.1044	ML
GS-T_{19}	4.05 (306)	0.0272	ML	MS1-T_{17}	4.03 (308)	0.0104	ML

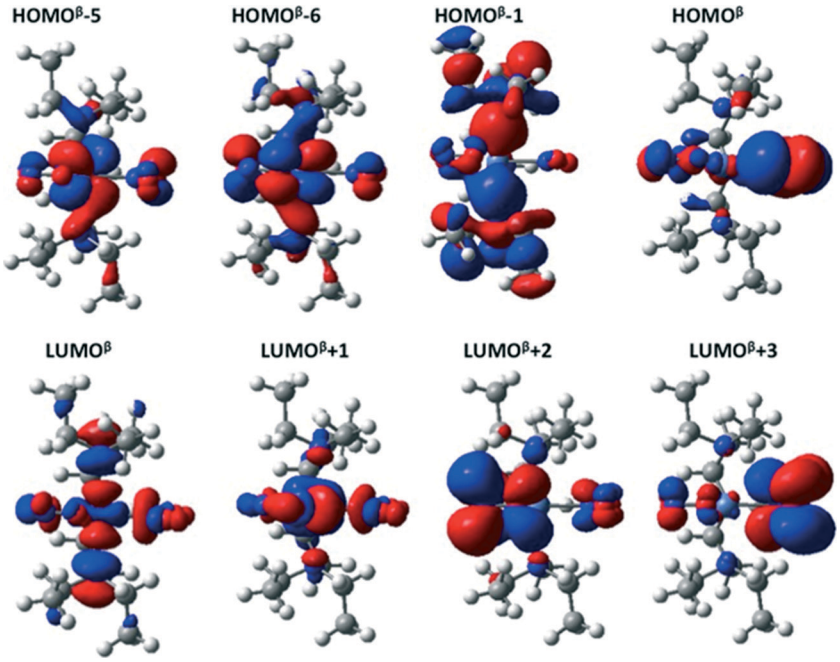

Fig. 6 Schematic of the molecular orbitals involved in the most important electronic transitions in the GS isomer, computed with the M06 functional and the LANL2DZ/6-311++G(d,p) basis set with water as a continuum. The labelling convention is based on the beta spin channel (that which does not contain the two unpaired electrons), in which the most important calculated electronic transitions take place.

plane and the p_y and p_z orbitals on the nitro ligands. Consequently, the Ni–N and Ni–O bonds weaken when these excited states are populated. Although these states are not directly populated during the photoabsorption, they most likely do play a role in the deactivation process – if the molecule behaves according Kasha's rule, it is expected to persist longest in the T_1 state.

For the GS molecule, the T_7, T_8 and T_{10} excited states are metal-to-ligand charge-transfer (MLCT) states, with the electron density transferred largely to the LUMO$^\beta$+2 and LUMO$^\beta$+3 orbitals, both of which are mainly localized on the NO_2 and ONO groups, respectively. The equivalent excited states in the MS1 complex are T_7, T_8, T_9 and T_{12}.

Around 3.6 eV, there are two excited states with oscillator strengths larger than 0.02, T_{11} and T_{12}, which both involve electronic transitions from the HOMO$^\beta$ to LUMO$^\beta$+1 orbitals, yielding a redistribution of electron density from the orbitals in the plane to those perpendicular to it. The brightest computed excited states appear around 4 eV, and are T_{17}–T_{19}(GS) and T_{15}–T_{17}(MS1). The main electronic transitions giving rise to these states are from the HOMO$^\beta$ and HOMO$^\beta$–1 to the LUMO$^\beta$ and LUMO$^\beta$+1 orbitals.

The photocrystallographic experiments in ref. 10 were performed irradiating at the absorption maximum at 400 nm, and also at 500 nm to allow for better penetration of the light into the crystal. In both cases, the photoisomerisation reaction occurs with good conversion.[7,10] These conditions should lead to population of excited states around T_{11}, plus vibrationally-excited states of higher-energy electronic configurations which could contain contributions from the brightest states (*e.g.* T_{18}). All these states lead to an increased antibonding interaction between the Ni and N atoms, which is consistent with their activating the GS → MS1 isomerisation.

To explore this further, we computed the excited states of all the species involved in the thermal isomerisation mechanisms. Photochemical processes typically involve multiple states, and crossing between states with different spin multiplicity can also be important; therefore, singlet as well as triplet excited states were considered. The energy difference between the ground-state triplet and singlet states for the GS species is 1.31 eV, and there are three triplet excited states lower in energy than the singlet ground state.

Fig. 7 shows the energy profiles for the lowest-energy GS → MS1 photoisomerisation pathway; data for the other pathways, including for the MS1 → MS2 transition, may be found in the ESI.† The calculated isomerisation barriers in the singlet state are of the same order of magnitude or higher than the corresponding triplet barriers. Since the singlet and triplet states near in energy have different character, and the coupling between singlets and triplets requires this difference in electronic nature,[47] plus a small energy difference to increase the spin–orbit coupling, crossing between singlet and triplets is a possibility which cannot be discarded; however, only a few singlet excited states are found below the corresponding triplets, which suggests crossings may not form a major part of the photochemical reaction mechanism.

Considering only the states with triplet multiplicity, three isomerisation mechanisms could potentially be important following light absorption: 1) isomerisation during the relaxation to T_1; 2) isomerisation once the system is in T_1; and 3) isomerisation in T_0 if the excitation energy is transferred into vibrations, and the isomerisation then happens in the vibrational hot-ground state (*i.e.* vibronic coupling). Considering that the key experimental observations can be explained based on ground-state calculations, the third mechanism seems to be a likely candidate. Nonetheless, since photoexcitation is expected to populate states with significant antibonding character between the metal and the ligand, isomerisation in the excited state is also a strong possibility.

It is also possible that the photochemical process could occur through a combination of all these mechanisms. To distinguish between them, non-adiabatic dynamics simulations would be required. At present, such simulations are rare for organometallic compounds, due to the complexity of their potential-energy surfaces, which typically contain a high density of excited states and crossings between states of different multiplicities.[45,48,49] This is an area of ongoing research that we aim to explore in our future work.

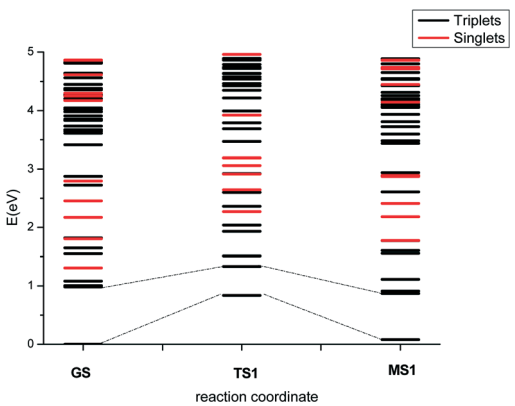

Fig. 7 Energy profiles for the GS → MS1 transition in the ground and photoexcited states. Triplet and singlet states are indicated by black and red lines, respectively. The excited states were computed at the TD-DFT/M06/LANL2DZ/6-311++G(d,p) level of theory with water as a continuum.

Conclusions

In summary, we have applied a combination of solid-state and molecular quantum-chemistry calculations to model the energetics and isomerisation processes in the [Ni(Et$_4$dien)(η^2-O,ON)(η^1-NO$_2$)] system.

The effect of the isomerisable ligand on the Ni 3d states and weak interactions between the ligand and the Et$_4$dien backbone appear to both be important contributors to the energy differences between the different linkage isomers. Our results suggest that the dielectric environment of the molecular crystal likewise has a significant effect on the relative stability of the isomers, and, to a lesser extent, the isomerisation barriers. However, beyond this the interactions between the molecular units in the solid are minimal, and thus polarisable-continuum model (PCM) calculations, with a suitable choice of the dielectric constant, may represent an efficient means of modelling this and, most likely, related systems.

Transition-state modelling suggests that the nitro-to-*endo*-nitrito and *endo*-to-*exo*-nitrito isomerisation scan both occur *via* rotations of the NO$_2$ ligand out of the plane formed by the Ni–NO$_2$ group in the (meta)stable isomers; the latter mechanism was verified by solid-state molecular dynamics, confirming the validity of this approach. There is an apparent overestimation of the activation barrier for the GS-to-MS1 transition compared to experiment, which requires further investigation; possibly in relation to this, we found no evidence of a transition path connecting the *exo*-nitrito and nitro forms directly, the reasons for which are not clear at present.

Modelling the photochemistry of the complex suggests that isomerisation could occur both in the electronically-excited state, and also in the vibrational hot-ground state after de-excitation. Distinguishing between these will require more involved non-adiabatic dynamics simulations, which will be a subject of further work. Furthermore, although

these pathways provide a plausible mechanism for the photochemical reaction, there are additional possibilities which merit further investigation (*e.g.* the possible role of other transient metastable species).

Overall, this modelling study has provided a comprehensive picture of the linkage isomerisation phenomenon in this system, and we hope that the insight we have obtained will provide a sound basis both for explaining the behaviour of known, related systems, as well as for designing new materials with tunable switching behaviour and properties. Future work on this system, and on the simulation of molecular crystals in general, will benefit from exploiting more fully the synergy between solid-state and molecular modelling.

Acknowledgements

Illustrations were generated with the assistance of A. J. Jackson. The authors gratefully acknowledge financial support from an EPSRC programme grant (grant no. EP/K004956/1) and the European Research Council (grant no. 277757). We acknowledge use of the HECToR and ARCHER supercomputers through membership of the UKs HPC Materials Chemistry Consortium, which is funded by EPSRC grant no. EP/F067496, in the completion of this work. We also acknowledge use of Hartree Centre resources in this work. The STFC Hartree Centre is a research collaboratory in association with IBM providing High Performance Computing platforms funded by the UK's investment in e-Infrastructure. The Centre aims to develop and demonstrate next generation software, optimised to take advantage of the move towards exa-scale computing.

Notes and references

1 L. E. Hatcher and P. R. Raithby, *Coord. Chem. Rev.*, 2014, DOI: 10.1016/j.ccr.2014.02.021.
2 U. Hauser, V. Oestreich and H. D. Rohrweck, *Z. Phys. A: At. Nucl.*, 1977, **208**, 17–25.
3 H. Zöllner, T. Woike, W. Krasser and S. Haussühl, *Z. Kristallogr.*, 1989, **188**, 130–153.
4 M. Rüdlinger, J. Schefer, G. Chevrier, N. Furer, H. U. Güdel, S. Haussühl, G. Heger, P. Schweiss, T. Vogt, T. Woike and H. Zöllner, *Z. Phys. B: Condens. Matter*, 1991, **83**, 125–130.
5 M. D. Carducci, M. R. Pressprich and P. Coppens, *J. Am. Chem. Soc.*, 1997, **119**, 2669–2678.
6 M. R. Warren, S. K. Brayshaw, A. L. Johnson, S. Schiffers, P. R. Raithby, T. L. Easun, M. W. George, J. E. Warren and S. J. Teat, *Angew. Chem.*, 2009, **121**, 5821–5824.
7 L. E. Hatcher, M. R. Warren, D. R. Allan, S. K. Brayshaw, A. L. Johnson, S. Fuertes, S. Schiffers, A. J. Stevenson, S. J. Teat, C. H. Woodall and P. R. Raithby, *Angew. Chem., Int. Ed.*, 2011, **50**, 8371–8374.
8 S. K. Brayshaw, T. L. Easun, M. W. George, A. M. E. Griffin, A. L. Johnson, P. R. Raithby, T. L. Savarese, S. Schiffers, J. E. Warren, M. R. Warren and S. J. Teat, *Dalton Trans.*, 2012, **41**, 90–97.
9 M. R. Warren, T. L. Easun, S. K. Brayshaw, R. J. Deeth, M. W. George, A. L. Johnson, S. Schiffers, S. J. Teat, A. J. Warren, J. E. Warren, C. C. Wilson, C. H. Woodall and P. R. Raithby, *Chem. – Eur. J.*, 2014, **20**, 5468–5477.
10 L. E. Hatcher, J. Christensen, M. L. Hamilton, J. Trincao, D. R. Allan, M. R. Warren, I. P. Clarke, M. Towrie, S. Fuertes, C. C. Wilson, C. H. Woodall and P. R. Raithby, *Chem. – Eur. J.*, 2014, **20**, 3128–3134.
11 P. Coppens, I. Novozhilova and A. Kovalevsky, *Chem. Rev.*, 2002, **102**, 861–883.
12 D. A. Johnson and V. C. Dew, *Inorg. Chem.*, 1979, **18**, 3273–3274.
13 A. Y. Kovalevsky, K. A. Bagley and P. Coppens, *J. Am. Chem. Soc.*, 2002, **124**, 9241–9248.
14 A. Y. Kovalevsky, K. A. Bagley, J. M. Cole and P. Coppens, *Inorg. Chem.*, 2003, **42**, 140–147.
15 A. E. Phillips, J. M. Cole, T. d'Almeida and K. S. Low, *Phys. Rev. B: Condens. Matter Mater. Phys.*, 2010, **82**, 155118.
16 W. Kohn and L. J. Sham, *Phys. Rev.*, 1965, **140**, 1133–1138.
17 G. Kresse and J. Hafner, *Phys. Rev. B: Condens. Matter Mater. Phys.*, 1993, 47.
18 L. A. Constantin, J. M. Pitarke, J. F. Dobson, A. Garcia-Lekue and J. P. Perdew, *Phys. Rev. Lett.*, 2008, 100.
19 J. P. Perdew, K. Burke and M. Ernzerhof, *Phys. Rev. Lett.*, 1996, **77**, 3865–3868.
20 S. Grimme, *J. Comput. Chem.*, 2006, **27**, 1787–1799.
21 S. Grimme, J. Antony, S. Ehrlich and H. Krieg, *J. Chem. Phys.*, 2010, 132.
22 M. Dion, H. Rydberg, E. Schroder, D. C. Langreth and B. I. Lundqvist, *Phys. Rev. Lett.*, 2004, 92.
23 K. Lee, E. D. Murray, L. Z. Kong, B. I. Lundqvist and D. C. Langreth, *Phys. Rev. B: Condens. Matter Mater. Phys.*, 2010, 82.
24 P. E. Blochl, *Phys. Rev. B: Condens. Matter Mater. Phys.*, 1994, **50**, 17953–17979.
25 S. L. Dudarev, G. A. Botton, S. Y. Savrasov, C. J. Humphreys and A. P. Sutton, *Phys. Rev. B: Condens. Matter Mater. Phys.*, 1998, **57**, 1505–1509.
26 H. J. C. Berendsen, J. P. M. Postma, W. F. Vangunsteren, A. Dinola and J. R. Haak, *J. Chem. Phys.*, 1984, **81**, 3684–3690.
27 M. J. Frisch, G. W. Trucks, H. B. Schlegel, G. E. Scuseria, M. A. Robb, J. R. Cheeseman, G. Scalmani, V. Barone, B. Mennucci, G. A. Petersson, H. Nakatsuji, M. Caricato, X. Li, H. P. Hratchian, A. F. Izmaylov, J. Bloino, G. Zheng, J. L. Sonnenberg, M. Hada, M. Ehara, K. Toyota, R. Fukuda, J. Hasegawa, M. Ishida, T. Nakajima, Y. Honda, O. Kitao, H. Nakai, T. Vreven, J. A. Montgomery, J. E. Peralta, F. Ogliaro, M. Bearpark, J. J. Heyd, E. Brothers, K. N. Kudin, V. N. Staroverov, R. Kobayashi, J. Normand, K. Raghavachari, A. Rendell, J. C. Burant, S. S. Iyengar, J. Tomasi, M. Cossi, N. Rega, N. J. Millam, M. Klene, J. E. Knox, J. B. Cross, V. Bakken, C. Adamo, J. Jaramillo, R. Gomperts, R. E. Stratmann, O. Yazyev, A. J. Austin, R. Cammi, C. Pomelli, J. W. Ochterski, R. L. Martin, K. Morokuma, V. G. Zakrzewski, G. A. Voth, P. Salvador, J. J. Dannenberg,

S. Dapprich, A. D. Daniels, Ö. Farkas, J. B. Foresman, J. V. Ortiz, J. Cioslowski and D. J. Fox, *Gaussian 09, Revision A.02. Gaussian, Inc.*, Wallingford CT, 2009.
28 C. Adamo and V. Barone, *J. Chem. Phys.*, 1999, **110**, 6158–6170.
29 A. D. Becke, *J. Chem. Phys.*, 1993, **98**, 1372–1377.
30 J. M. Tao, J. P. Perdew, V. N. Staroverov and G. E. Scuseria, *Phys. Rev. Lett.*, 2003, 91.
31 Y. Zhao and D. G. Truhlar, *Theor. Chem. Acc.*, 2008, **120**, 215–241.
32 T. Yanai, D. P. Tew and N. C. Handy, *Chem. Phys. Lett.*, 2004, **393**, 51–57.
33 Y. Zhao and D. G. Truhlar, *Acc. Chem. Res.*, 2008, **41**, 157.
34 J. Tomasi, B. Mennucci and R. Cammi, *Chem. Rev.*, 2005, **105**, 2999–3093.
35 H. P. Hratchian and H. B. Schlegel, *J. Chem. Phys.*, 2004, **120**, 9918–9924.
36 Y. Zhao and D. G. Truhlar, *J. Phys. Chem. A*, 2006, **110**, 5121–5129.
37 Y. Zhao and D. G. Truhlar, *J. Phys. Chem. A*, 2006, **110**, 13126–13130.
38 J. D. Chai and M. Head-Gordon, *Phys. Chem. Chem. Phys.*, 2008, **10**, 6615–6620.
39 I. A. Vladimir, F. Aryasetiawan and A. I. Lichtenstein, *J. Phys.: Condens. Matter*, 1997, **9**, 767.
40 A. B. Shick, A. I. Liechtenstein and W. E. Pickett, *Phys. Rev. B: Condens. Matter Mater. Phys.*, 1999, **60**, 10763–10769.
41 M. Cococcioni and S. de Gironcoli, *Phys. Rev. B: Condens. Matter Mater. Phys.*, 2005, 71.
42 A. E. Reed, L. A. Curtiss and F. Weinhold, *Chem. Rev.*, 1988, **88**, 899–926.
43 G. C. Pimentel and A. L. McClellan, *The hydrogen bond. (Drawings by Roger Hayward.)*, Reinhold Publishing Corporation, New York 22, 1963.
44 W. Humphrey, A. Dalke and K. Schulten, *J. Mol. Graphics Modell.*, 1996, **14**, 33–38.
45 R. Crespo-Otero and M. Barbatti, *J. Chem. Phys.*, 2011, **134**, 164305.
46 D. Escudero and W. Thiel, *J. Chem. Phys.*, 2014, **140**, 194105.
47 S. K. Lower and M. A. El-Sayed, *Chem. Rev.*, 1966, **66**, 199–241.
48 L. Freitag and L. González, *Inorg. Chem.*, 2014, **53**(13), 6415–6426.
49 I. Tavernelli, B. F. E. Curchod and U. Rothlisberger, *Chem. Phys.*, 2011, **391**, 101–109.

